Desalination and Water Treatment
www.deswater.com

doi: 10.5004/dwt.2020.25319

184 (2020) 326–339
April

Biomass-derived magnetically tuned carbon modified Sepiolite for effective removal of Congo red from aqueous solution

Shappur Vahidhabanu[a,b,*], Irulappan Swathika[a,b], Abideen Idowu Adeogun[a,c], Ramakrishnan Roshni[a,b], B. Ramesh Babu[a,b,*]

[a]*CSIR-Central Electro Chemical Research Institute, Pollution Control Division, Karaikudi – 630003, Tamil Nadu, India, Tel. +91-4565-241441; Fax: +91-4565-227779; email: vahishappur@gmail.com (S. Vahidhabanu), brbabu@cecri.res.in (B.R. Babu)*
[b]*Academy of Scientific and Innovative Research (AcSIR), Ghaziabad – 201002, India*
[c]*Chemistry Department, Federal University of Agriculture, Abeokuta, Nigeria*

Received 10 June 2019; Accepted 5 December 2019

ABSTRACT

Biomass-derived carbon-based magnetic tuned Sepiolite nanocomposite, Fe_3O_4-Sepiolite/C was synthesized and characterized using scanning electron microscopy, energy-dispersive X-ray analysis, X-ray diffraction, vibrating sample magnetometer, Fourier transform infrared spectroscopy as well as atomic force microscopy techniques. The adsorbent was used for adsorption removal of Congo red dye from synthetic wastewater in a batch process, the effects of operating parameters such as; initial concentrations (10–50 ppm), contact time (0–240 min) and pH were investigated. Data from the kinetic study were analyzed with pseudo-first-order and pseudo-second-order, while the mechanism was analyzed using Elovich and intra-particle diffusion models. The equilibrium data were evaluated using Langmuir, Freundlich, Temkin, and Dubinin–Radushkevich isotherm models. The adsorption kinetics of the dye removal followed pseudo-first-order with constant rate increases from 0.031 to 0.068 min^{-1} as the initial concentration increases from 50 to 200 mg L^{-1}. Equilibrium data fitted well with all the isotherm data were investigated, the Langmuir model showed that the maximum adsorption capacities of the adsorbent were 199.0 mg g^{-1}. The negative $\Delta G°$ values obtained from thermodynamic studies showed that the adsorption spontaneous, while positive $\Delta H°$ value of 6.549 kJ mol^{-1} and entropy change $\Delta S°$ revealed an increased activity at the solid/liquid interface. The results obtained from this study showed that Fe_3O_4-Sepiolite/C is an excellent adsorbent with good surface morphology and magnetic property for effective removal of Congo red dye from an aqueous solution and recyclability.

Keywords: Sepiolite; Magnetic; Biomass; Congo red; Adsorption; Isotherms; Kinetics

1. Introduction

Adsorption is a highly efficient and low-cost technique for the removal of pollutants from wastewaters even at low concentrations [1]. Activated carbons have been widely used in wastewater treatments to remove inorganic or organic pollutants because of their huge specific surface area, high adsorption capacity rate, and surface reactivity [2–4]. However, some drawbacks of sluggish adsorption kinetics and limited adsorption capacity for the removal of organic contaminants had been reported [5], also activated carbon regeneration typically involves drying at elevated temperature, that is., costly and causes partial destruction of this material [6]. Hence, the need to search for alternative materials and the development of advanced technologies to remediate past contamination and prevent further environmental degradation.

* Corresponding authors.

Adsorption of reactive dye into various adsorbents has been a subject of discussion in recent times. Sewage sludge [7], cellulose [8], agriculture residues [9–11] and natural clay [12–15] had been reported to be effective adsorbents for dyes removal.

Clay minerals, the main component of the mineral fraction of soils as well as agricultural waste biomass are some of the cheap and natural materials that are abundant in nature [16]. Apart from the environmental problems, misuse of the biomass materials constitutes loss of potentially valuable resources. Annually, about 140 billion metric tons of waste biomass is generated solely from agricultural activities globally, its ineffective disposal constitutes huge problem while their decomposition generates greenhouse gases that contribute to the global climate change [17]. Agricultural waste biomass is rich in cellulose, which can be converted into porous carbon, synthesis of functional carbon-based nanomaterials from biomass via hydrothermal carbonization process had been reported [18–22]. Similarly, clay minerals have demonstrated effectiveness as natural adsorbents due to their small particle sizes, lamellar structures, and negatively charged surfaces, which make them good cation adsorbents with large reactive surface areas for ion exchange or electrostatic attraction [23].

Sepiolite is a clay mineral with a unique fibrous structure [24] which confers it a large specific surface area and high adsorption capacity, hence, its wide application in the field of adsorption for wastewater treatment, among others [25]. Nevertheless, the adsorption capacity of raw Sepiolite is limited and its performance as adsorbent could be significantly improved and regeneration could also be impacted when functionalized. Combining the surface properties of carbon adsorbent and the need to recycle and recover adsorbent from the solution, a clay composite of carbon with magnetic support will be of interest.

In this study, therefore, corncob was used as a carbon precursor for the synthesis of a novel magnetic-Sepiolite/carbon nanocomposite (Fe_3O_4-Sepiolite/C). The composite was used as an adsorbent for removal of Congo red dye from aqueous media. The effect of adsorption parameters such as pH, adsorbent concentration, contact time, initial dye concentration as well as temperature was investigated while the kinetic and equilibrium data were analyzed to elucidate the adsorption process.

2. Materials and method

2.1. Materials

Corncob was obtained from a local farmer at Alagappapuram, Karaikudi, Tamil Nadu, Sepiolite clay, polytetrafluoroethylene (PTFE), iron (III) chloride hexahydrate ($FeCl_3{\cdot}6H_2O$) and iron (II) chloride tetrahydrate ($FeCl_2{\cdot}4H_2O$) (AR grade) were products of Sigma-Aldrich (St. Louis, Missouri, United States). Ammonium was from ACS Emsure Reagents (Ahmedabad - 380013, Gujarat, India), while hydrochloric acid and sodium hydroxide were procured from Merck, India. Congo red dye was a product of Loba Chemicals, India. Other reagents were analytical grade and Milli-Q water was used for all of the experiments.

Corncobs were washed under running tap to remove dirt, cut into smaller pieces and dried overnight at 105°C. The dried pieces were further pulverized, sieved to obtain particle size less than 150 μm, the sample was then stored in an airtight container until needed. Sepiolite was activated by washing 10 g of the clay with Milli-Q water and acid-treated with concentrated HCl (0.8 mol L^{-1}) for 4 h, then washed several times to neutral pH with Milli-Q water and dried at 105°C for 2 h.

2.2. Synthesis of magnetic nanoparticle

The magnetic nanoparticle was prepared by dissolving 4.8 g of $FeCl_3{\cdot}6H_2O$ and 1.8 g of $FeCl_2{\cdot}4H_2O$ in 75 ml of deionized water under constant stirring for 30 min, ammonium solution 25 ml was added to adjust the pH about 11. The residue was separated using an external magnetic field and washed thrice each with ethanol and water, finally separated by centrifugation for 10 min.

2.3. Synthesis of Fe_3O_4-Sepiolite/C nanocomposite

Corncob was used as a carbon precursor, 1 g of the powder was mixed with 2.56 g of PTFE and 8 g of Sepiolite clay, the mixture was transferred into an agate mortar and mixing was continued for further 30 min. The resulting mixture was transferred into a microwave oven at 600 W about 10 min under N_2 at a flow rate of at 2 L/min. The sample obtained was labeled as Fe_3O_4-Sepiolite/C.

2.4. Characterization

The morphology and elemental composition of the Fe_3O_4-Sepiolite/C was investigated using scanning electron microscopy (Hitachi, Japan, S-3000H) equipped with energy-dispersive X-ray (EDX), Further characterizations were carried out using transmission electron microscopy (TEM; Tecnai 20 G2 FEI, 186, The Netherlands) analysis with the selected-area electron diffraction (SAED) pattern taken. Also, atomic force microscopy (AFM) Agilent technologies (model 5500) was used for topographic studies, while X-ray diffraction (XRD) pattern of these samples was obtained using X-ray diffractometer (PANalytical X'Pert PRO, The Netherland) using CuKα (γ = 1.54178 Å) radiation. Fourier transform infrared (FTIR) spectra were recorded from 400 to 4,000 cm^{-1} in the TENSOR 27 spectrometer (Bruker, Germany) using the KBr pellet technique. The magnetic properties of the Fe_3O_4 and Fe_3O_4-Sepiolite/C composite were characterized by a Physical Property Measurement System (PPMS, Dynacool, Quantum Design).

2.5. Preparations of aqueous solution of the dye

The stock solution containing Congo red dye (Fig. 1) was prepared by dissolving accurately weighed solute such that the solution contained 1 g equivalent of the dye in 1 L Milli-Q water, working standard solutions were prepared from the stock by dilution. The pH of the working solution was maintained with an aliquot of HCl or NaOH prior to the adsorption study.

2.6. Adsorption studies

The batch equilibrium and kinetics adsorption studies were conducted in process in Erlenmeyer flasks containing

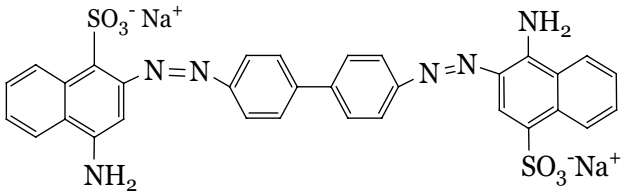

Fig. 1. Structure of Congo red dye.

25 mL of dye solutions with a concentration range between 50–200 mL^{-1} and 0.4 g L^{-1} of the adsorbents. The contents were placed in a regulated water bath (30°C ± 1°C) with shaker at 150 rpm, samples were collected at pre-set time intervals and the dye concentrations in aqueous media were by reading the absorbance at 497 nm on UV-vis spectrophotometer (UV-VIS-NIR VARIAN 500 Scan CARY). The amount of dye adsorbed (mg g^{-1}) by the adsorbents as a function of time (Q_t) and at equilibrium (Q_e) was estimated according to Eqs. (1) and (2):

$$Q_t = \frac{(C_0 - C_t)}{m} V \quad (1)$$

$$Q_e = \frac{(C_0 - C_e)}{m} V \quad (2)$$

where C_0, C_t and C_e are the initial, time t and equilibrium concentrations (mg L^{-1}) of the dye respectively, V is the volume (L) of the solution and m is the mass (g) of the adsorbent.

3. Result and discussion

3.1. Characterization of the adsorbent

The surface morphology of Sepiolite, corncob, corncob carbon, and Fe_3O_4-Sepiolite/C were observed with a scanning electron microscope, Fig. 2a reveals a stone-like aggregate fiber of Sepiolite, Fig. 2b also shows the rough surface of corncob before its conversion to carbon with reduced particle size and increase surface area (Fig. 2c). The surface morphology of Fe_3O_4-Sepiolite/C (Fig. 2d) revealed a distinct surface different from the precursors. The fibrous structures of the Sepiolite had become distorted and transformed to 3-D morphologies as carbon and Fe_3O_4 were incorporated into the composite, similar observations had earlier been reported [23].

EDX analysis of the Sepiolite, raw corncob, corncob carbon, and Fe_3O_4-Sepiolite/C are shown in Fig. 3. Sepiolite is a natural clay mineral rich in magnesium and silica as shown in Fig. 3a, the corncob is also rich in carbon and oxygen due to its cellulosic nature (Figs. 3b and c), while the EDX of the composite (Fig. 2d) showed that the carbon and Fe_3O_4 had been incorporated into the Sepiolite.

The microscopic structure of the Sepiolite and Fe_3O_4-Sepiolite/C observed with high-resolution transmission

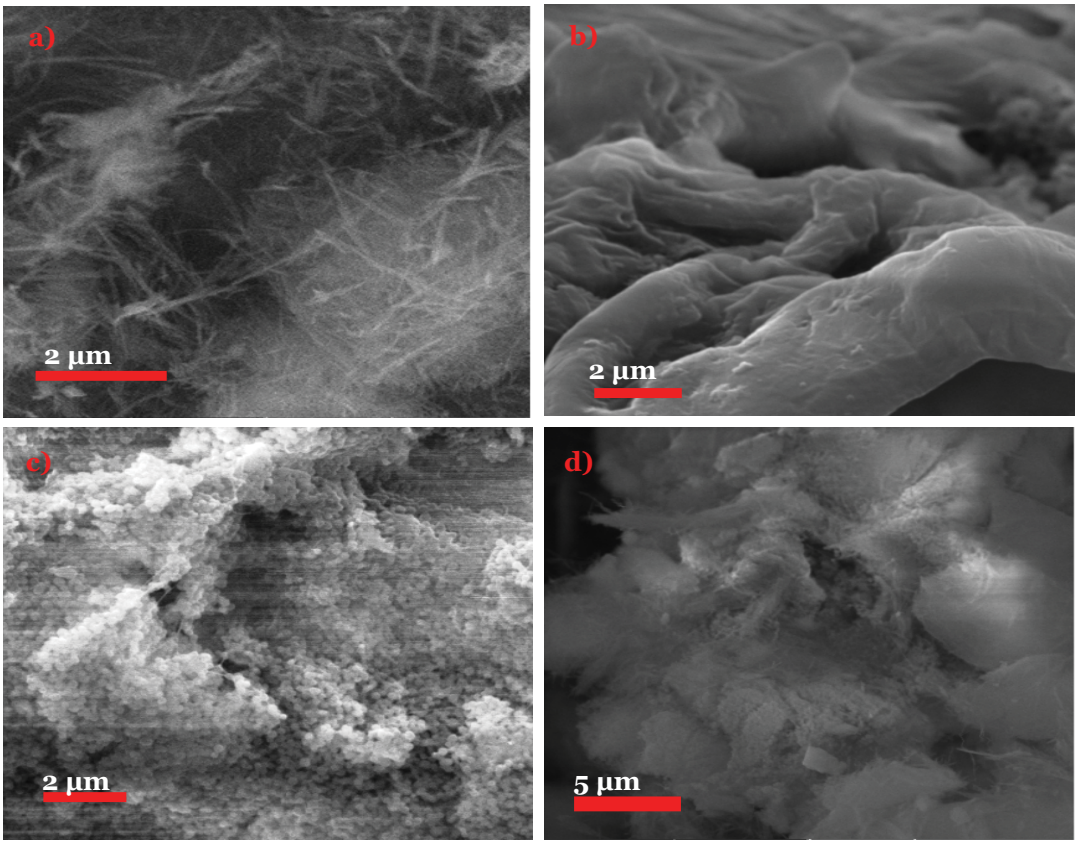

Fig. 2. Scanning electron microscopy images of (a) raw Sepiolite, (b) raw corncob, (c) corncob carbon, and (d) Fe_3O_4-Sepiolite/C.

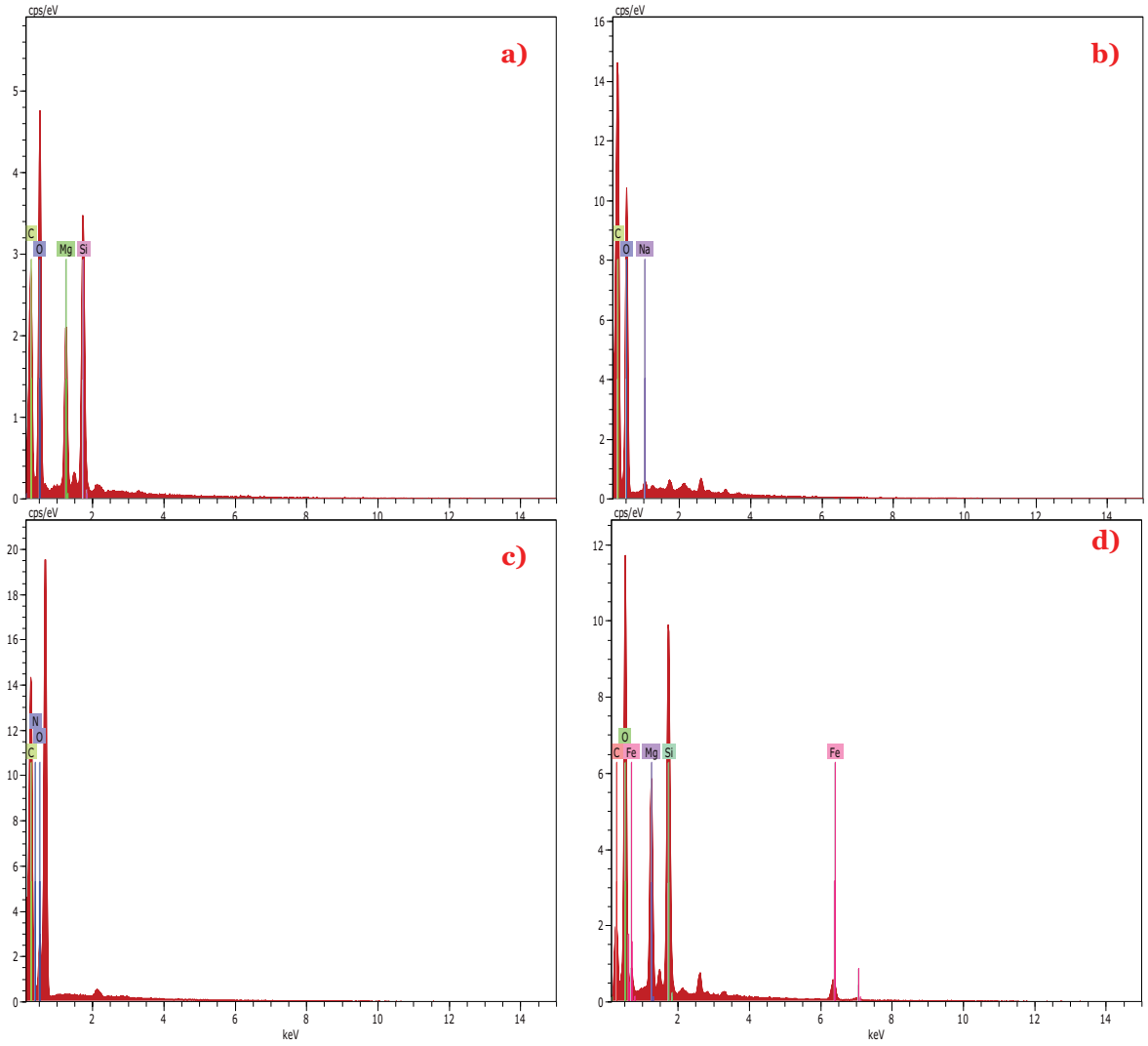

Fig. 3. EDX analysis of (a) raw Sepiolite, (b) raw corncob, (c) corncob carbon, and (d) Fe_3O_4-Sepiolite/C.

electron microscopy (HRTEM) revealed that Sepiolite (Fig. 4a) is made up of rod-like nanoparticles with a particle size of 28–50 nm in length and 10–15 nm in width with SAED pattern suggesting a crystalline structures. However, the image obtained from the composite analysis (Fig. 4b) revealed that the clay had been modified, the rod-like structure had been coated with the other composites and the surface structure appeared denser. The structure of the Sepiolite could still be seen as grey sticks under the white part, it is obvious that the size has changed with the improved surface as indicated by SAED.

The topography and deflection of the composites were obtained from AFM analysis and the results are shown in Fig. 5. Fe_3O_4 morphology is displayed in Fig. 5a, the surface was noticed to be smooth with uniform diameters of about 14.2 nm. Sepiolite (Fig. 5b) analysis revealed a rough surface with a thickness of about 25.5 nm while the Fe_3O_4-Sepiolite/C, Fig. 5c shows a very rough surface with a thickness of about 32.5 nm. The surface roughness obtained from the roughness profiles express as R_a-value (mean deviation of roughness profile) is in the order of 0.608, 0.809, and 3.07 nm for Fe_3O_4, Sepiolite, and Fe_3O_4-Sepiolite/C respectively. This is a clear indication that surface modification had an impact on the roughness of the surface with pores [26].

XRD spectra of corncob powder, its carbon, raw Sepiolite, and Fe_3O_4-Sepiolite@C are presented in Fig. 6. The broad peaks at 2θ values of about 23.1° and 35.5° were noticed in the diffraction spectra corncob powder which is an indication of its amorphous nature. The XRD pattern of the carbon from the biomass show sharp peaks at 2θ values of about 18.3°, 31.9°, and 37.2° with partial retention of the broad peak at 23.1°, the difference can be attributed to the material structural reordering [27]. The XRD pattern of the Fe_3O_4-Sepiolite@C displayed all the characteristics of the components, the majority of the peak of the raw Sepiolites were displayed while those of the carbon was also incorporated, this also confirmed the results of the TEM analysis. Distinct peaks at 2θ values of about 30.8°, 35.13°, and 44.5° are characteristics of Fe_3O_4 indicating that the composite had been magnetically incorporated [28].

Magnetic properties of Fe_3O_4-Sepiolite@C and Fe_3O_4 are compared in Fig. 7, an increase magnetization with a rise in the magnetic field was noted. The magnetic hysteresis loops

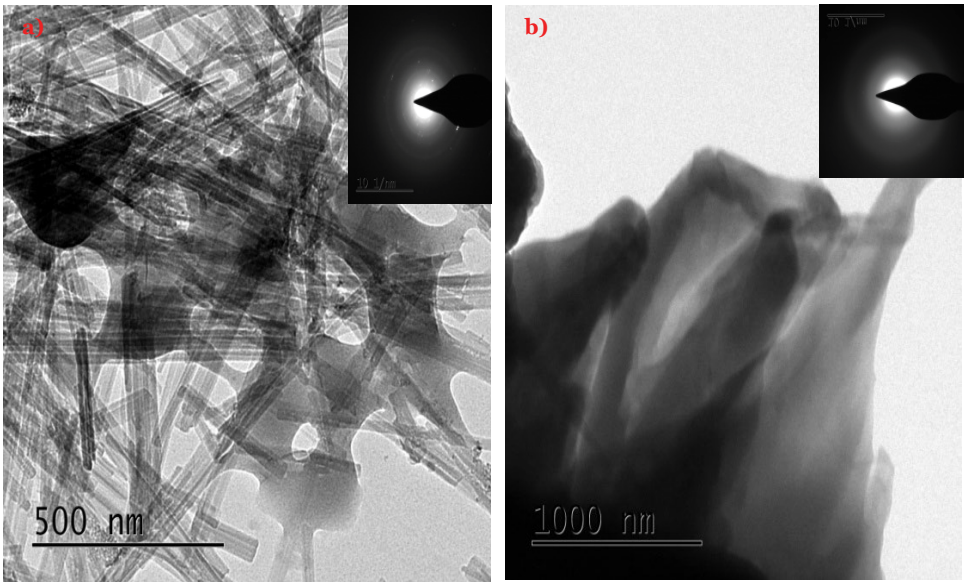

Fig. 4. HRTEM images of (a) raw Sepiolite and (b) Fe_3O_4-Sepiolite/C.

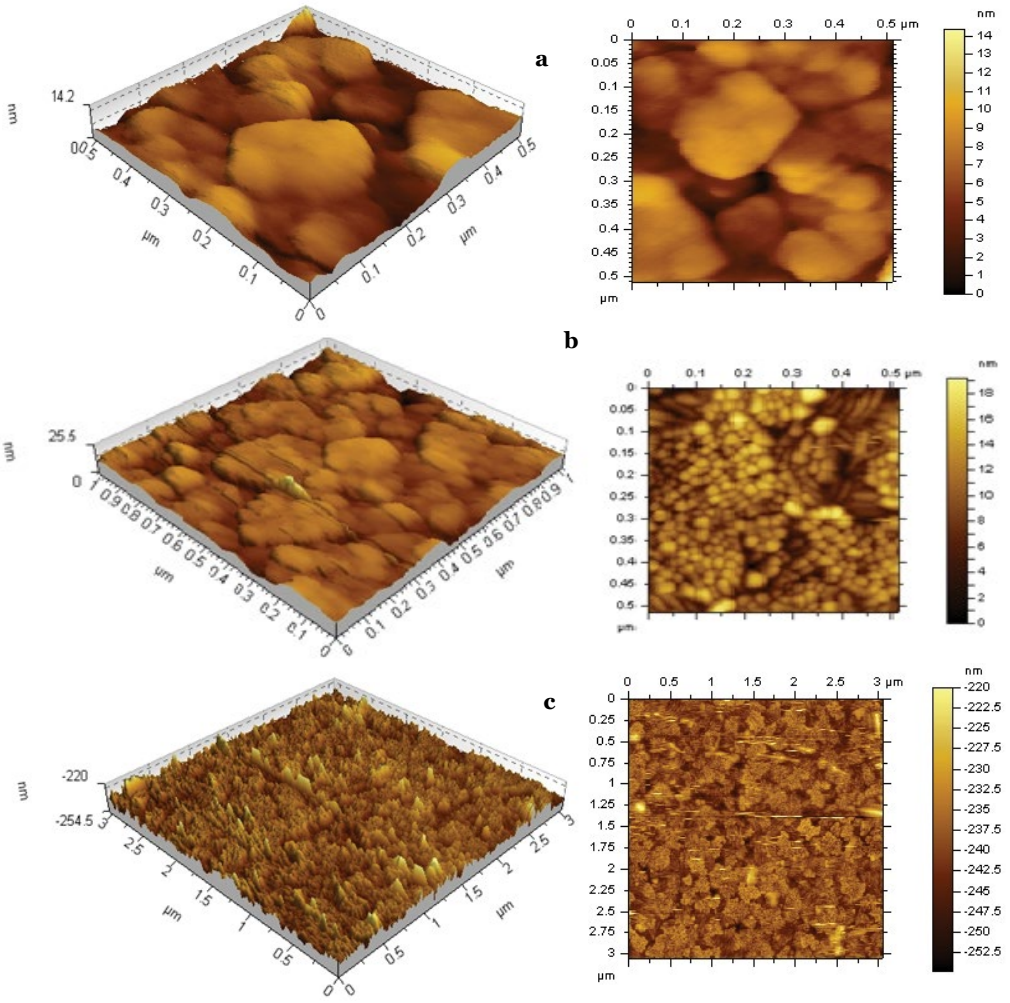

Fig. 5. AFM Images of Fe_3O_4-Sepiolite/C (a) Fe_3O_4, (b) Sepiolite, and (c) Fe_3O_4-Sepiolite/C.

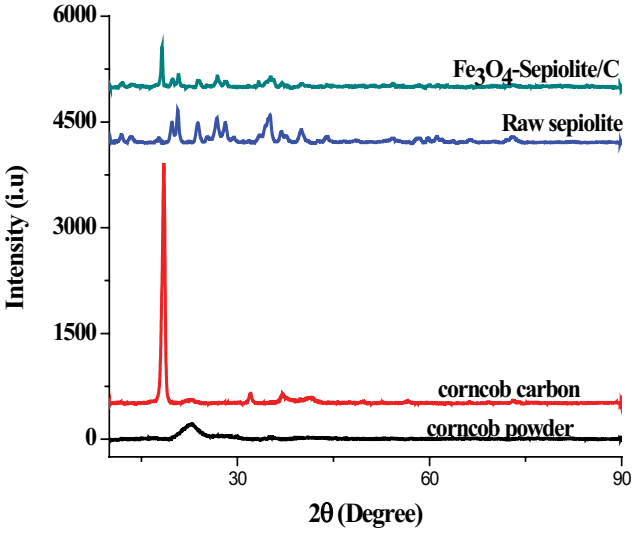

Fig. 6. XRD spectra corncob powder, its carbon, raw Sepiolite, and Fe_3O_4-Sepiolite@C.

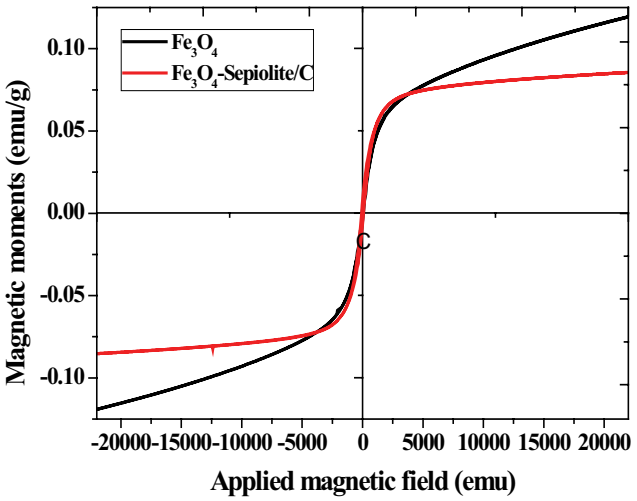

Fig. 7. Magnetic properties of Fe_3O_4-HNT/CTS composite.

are symmetrical through the origin with zero coercivity and remanence confirming the superparamagnetic property Fe_3O_4-Sepiolite@C [29,30]. The saturation magnetization of the Fe_3O_4-Sepiolite@C is lower than that of Fe_3O_4 with magnetization as a result of the presence of a larger portion of non-magnetic materials in the Fe_3O_4-Sepiolite@C.

The FTIR spectra of carbon, Sepiolite, and Fe_3O_4-Sepiolite/C before and after the adsorption are presented in Fig. 8. The broadband between 3,600 and 3,000 cm^{-1} may be attributed to O–H of the entrapped water while that at 2,900 cm^{-1} could be attributed to CH stretching, the broadband around 1,000 cm^{-1} is also due to CH bending. In the case of Sepiolite, the weak band observed at 3,600 cm^{-1} and above could be attributed to stretching vibration of the OH of the Mg–OH, the weak band below 3,000–3,600 cm^{-1} could be assigned to H–O–H at the surface of Si–O while that at 1,662 cm^{-1} is assigned to bending vibration of attached water molecule.

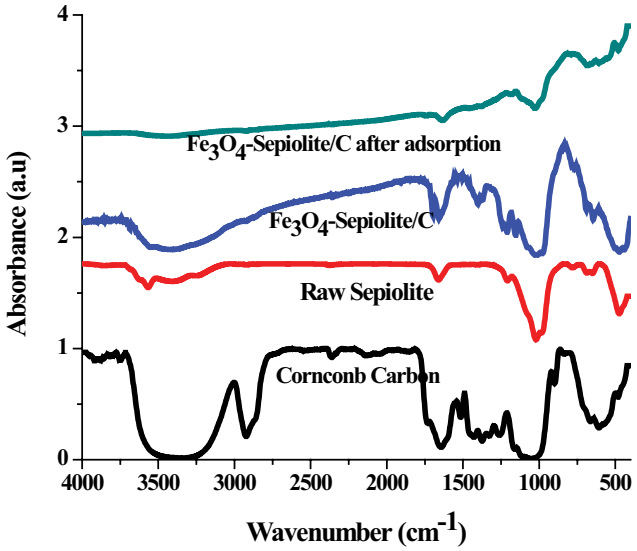

Fig. 8. FTIR spectra of carbon, Sepiolite, and Fe_3O_4-Sepiolite/C before adsorption and after adsorption.

The FTIR spectrum of Fe_3O_4-Sepiolite/C displayed prominent bands at 3,400 and 1,662 cm^{-1} which could be assigned to vibration bending and stretching of O–H, the band at 986 and 782 cm^{-1} can be related to in-plane bending of surface hydroxyl groups in Fe–OH– Fe. In addition, the band at 3,144 cm^{-1} is related to the stretching mode of Fe–O–OH. The functional group assignment are similar to those earlier reported [24,25] After adsorption of CR by Fe_3O_4-Sepiolite/C shift in band position, broadening and total disappearance of some peaks were noticed as shown in Fig. 5, this is an indication of interaction between the dye molecule and the functional groups present at the surface of the adsorbent.

3.2. Effects of contact time and initial concentrations on adsorption capacities

Evaluation of the influence of contact time at different initial dye concentrations enables the establishment of the equilibrium time for maximum dye uptake and determination of the adsorption process kinetic [31]. The adsorption rates rose rapidly with an increase in contact time as shown in Fig. 9, probably due to the presence of accessible sites on the adsorbent for interaction with the dye molecule, however, as the process progress, the rate became much slower possibly by the occupation of available sites. This brings about two phases noted in the figure, the rapid process lasted for between the first 20 and 30 min of the process after which the process assumed equilibrium and the adsorption rate proceeded steadily. Similar trends observed at each concentration suggests that the adsorption is concentration-dependent, as the initial dye concentration increases there was a corresponding increase in the adsorbed quantity of CR per unit mass of adsorbent when the dye concentration was increased from 50 to 200 mg L^{-1} the amount of adsorption quantity at equilibrium increased from 7.54 to 28.67 mg g^{-1}. This is due to increase driving force across the surface of the Fe_3O_4-Sepiolite/C as the dye concentration increases.

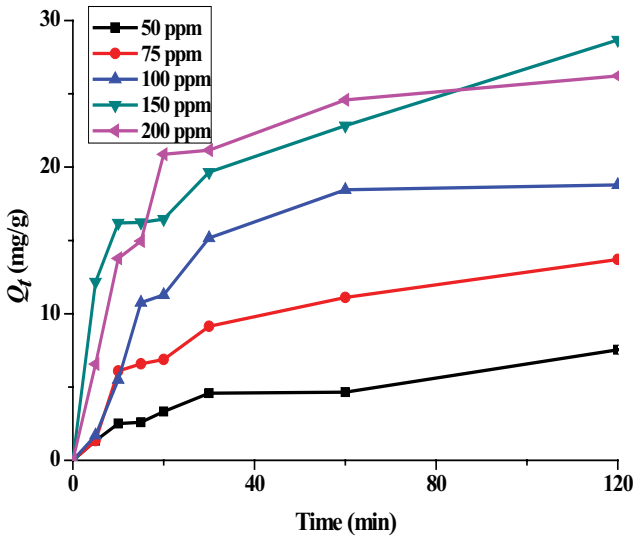

Fig. 9. Effects of contact time and initial concentrations on adsorption of CR by Fe_3O_4-Sepiolite/C.

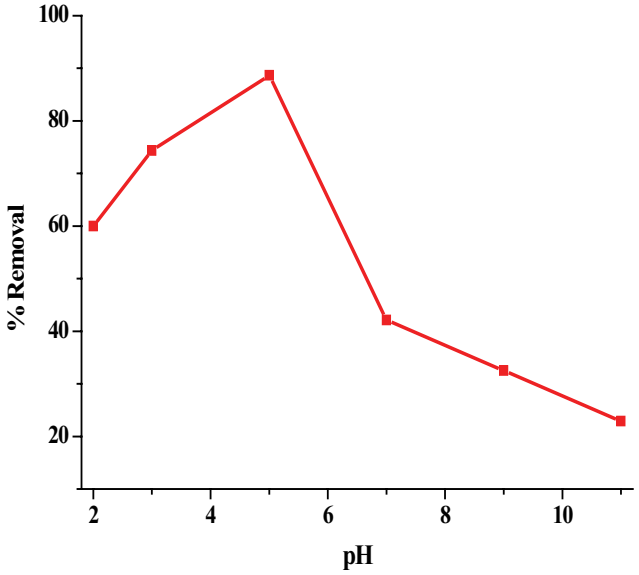

Fig. 10. Effects of pH adsorption of CR by Fe_3O_4-Sepiolite/C.

3.3. Effect of pH on removal efficiency of the adsorbent

Adsorption process to a certain extent depends on the pH of the medium because the interaction of the adsorbent and adsorbing species depends on the state at which they exist in the medium. Fig. 10 depicts the effect of pH on the efficiency of Fe_3O_4-Sepiolite/C for the removal of CR with pH. The removal efficiency increases with an increase in pH from 60% at pH 2 to 92% at an optimum pH of 6. This behavior may be as a result of the association of dye anions with the positively charged sites of Fe_3O_4-Sepiolite/C. Under the basic conditions, electrostatic repulsion between the negatively charged surface and dye molecules predominated leading to decrease adsorption capacity with an increase in pH.

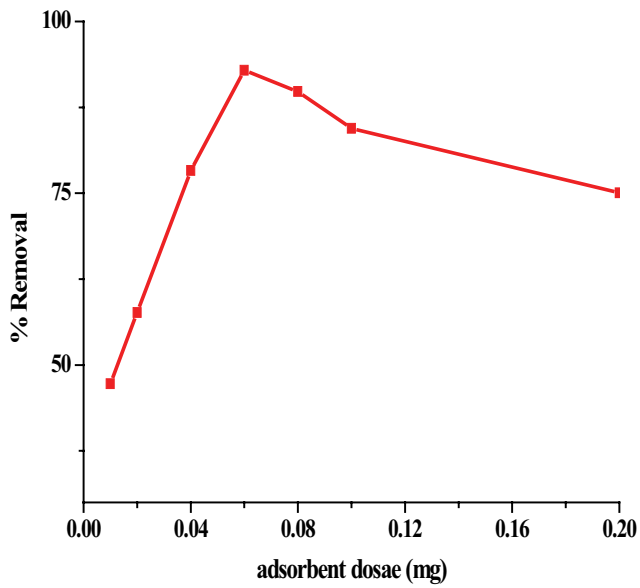

Fig. 11. Effects of adsorbent dosage adsorption of CR by Fe_3O_4-Sepiolite/C.

3.4. Effect of adsorbent dosage on removal efficiency

The effect of adsorbent dosage on the removal efficiency of CR by Fe_3O_4-Sepiolite/C is shown in Fig. 11. The removal efficiency of CR by Fe_3O_4-Sepiolite/C increased rapidly from 47.27% to 92.89% as the adsorbent dosage increases from 0.01 to 0.06 g. A further increase in adsorbent dosage doesn't have a corresponding effect rather a decrease in capacity was noted. The increase in the quantity of adsorbent leads to fluctuation in the available site resulting in increase adsorption efficiency as observed in the study. However, beyond a certain amount, a saturation of adsorption site due to the interaction of particle resulting in percolation or aggregation will lead to a reduction in available sites, reduced pore sizes and an increase in diffusional path length [31].

3.5. Adsorption kinetics studies

The adsorption rate at the solid/solution interface is best described using several kinetic models, data obtained from kinetics studies were subjected to the least square fits of some of these models. To elucidate the mechanism and the potential removal rate of the dye, the pseudo-first-order, and pseudo-second-order kinetic model were applied. The diffusion rate-controlling steps affecting the surface reaction were investigated to properly recognize the adsorption kinetics using intra-particle diffusion model while the Elovich kinetic model was used to characterize the effect of activated chemisorption on the adsorption kinetics. The mathematical expressions of these models (Eqs. (3)–(6)) are as presented in Table 1. Three error functions (Eqs. (5)–(7)), the sum square error function (SSE), root mean square error (RMSE) and composite fractional error (HYBRD) was applied to confirm the kinetic models fitting, (where N is the number of data, P is the number of parameters). The lower values of SSE, RMSE and HYBRD errors and the higher the value of R^2 the better the fitting of the model [33].

Table 1
Kinetic model for the adsorption studies of CR removal by Fe_3O_4-Sepiolite/C

Name	Model	Reference
Pseudo-first-order	$Q_t = Q_e\left(1-e^{-k_1 t}\right)$ (3)	[34]
	Q_e and Q_t are the amounts (mg g^{-1}) of dye adsorbed per unit mass of adsorbent at equilibrium time and time t, respectively, while k_1 (min^{-1}) is the rate constant for the pseudo-first-order kinetics.	
Pseudo-second-order	$Q_t = \frac{k_2 Q_e^2 t}{1+k_2 Q_e t}$ (4)	[35]
	Q_e and Q_t are the amounts (mg) of dye adsorbed per unit mass of adsorbent at equilibrium time and time t, respectively, while k_2 (g mg^{-1} min^{-1}) is the rate constant for the pseudo-second-order kinetics.	
Elovich	$Q_t = \frac{1}{\beta}\ln\left(\alpha\beta\times t\right)$ (5)	[36]
	where α (mg g^{-1}) is the initial adsorption rate constant and the parameter β (g mg^{-1} min^{-1}) is related to the extent of surface coverage and activation energy for chemisorptions.	
Intraparticle diffusion	$Q_t = K_{id} t^{0.5} + Ci$ (6)	[37]
	where K_{id} is the intraparticle diffusion rate constant (g mg^{-1} $min^{-0.5}$), and C is a constant (mg g^{-1}) which gives information about the thickness of the boundary layer.	

$$SSE = \sum_{i=1}^{N}\left(Q_{exp} - Q_{cal}\right)^2 \quad (7)$$

$$RMSE = \sqrt{\frac{1}{N-2}\sum_{i}^{N}\left(Q_{exp} - Q_{cal}\right)^2} \quad (8)$$

$$HYBRD = \frac{100}{N-P}\sqrt{\sum_{i=1}^{N}\left(\frac{\left(Q_{exp} - Q_{cal}\right)}{Q_{exp}}\right)^2} \quad (9)$$

Kinetic model fits for the removal of CR by Fe_3O_4-Sepiolite/C are presented in (Fig. 12a–d) while the corresponding parameters are also shown in Table 2. Pseudo-first-order adsorption kinetics displayed correlation coefficient R^2 ranging between 0.977 and 0.996 with the experimental values of Q_e at par with the calculated values at all concentrations investigated, the pseudo-second-order parameter, on the other hand, have R^2 ranged between 0.985 and 0.995 but the experimental values of Q_e differ slightly from the calculated values when compared with what was obtained from pseudo-first-order. The overall analysis of the error functions showed that the adsorption process for this adsorbent is best explained by the pseudo-first-order kinetic model. The rate constants k_1 is increases with increasing concentration, this may be a result of increased electrostatic interactions between the adsorbent and dye molecule as the increased driving forced the molecule into the pores and increase the diffusion gradients towards the adsorbent.

Fig. 12c shows that the Elovich model fitted the kinetic data satisfactorily given the values of R^2 and the error functions, the parameters revealed decrease in the value of β (a factor related to surface coverage) with corresponding increase α (adsorption rate) as the CR concentration increases which could be attributed to the decrease in surface activation energy with dye concentration. The intraparticle diffusion model fits is shown in Fig. 12d for further understanding of the mechanism of adsorption of CR on Fe_3O_4-Sepiolite/C. The adsorption process is best described by two steps mechanism, as confirmed by the intraparticle diffusion model, the first is the rapid process which lasted for the first 20 min, while the other part was the steady-state that led to the equilibrium. The corresponding parameters in the Table indicated a high correlation coefficient (R^2) suggesting a better fit. The parameters obtained for the fits indicated that the curves do not pass through the origin, that is, $C_1 \neq 0$, this is a confirmation that although the process involved intraparticle diffusion, it is not the sole rate-controlling step. The process could be described as having the first step of rapid dye uptake involving external and internal diffusion followed by prevailing slow step controlled by intraparticle diffusion mechanism until equilibrium was reached.

3.6. Adsorption isotherms

The equilibrium adsorption isotherms studies give parameters that are essential to explain the basic properties of adsorbent and the interactions with the adsorbing molecules. These are essential to the designing, understanding and optimization of the adsorption process. In addition, isotherm data are the basis for predicting and comparing the adsorption performance, it can be used for estimation of the adsorption mechanism pathways, estimation of the adsorbents capacities and effective designing of the adsorption systems. In this study, four common adsorption isotherm models namely, Langmuir, Freundlich, Temkin, and Dubinin–Radushkevich isotherm were applied to the adsorption equilibrium data, the isotherm parameters were obtained by the least square fit method as earlier mentioned. The mathematical expressions

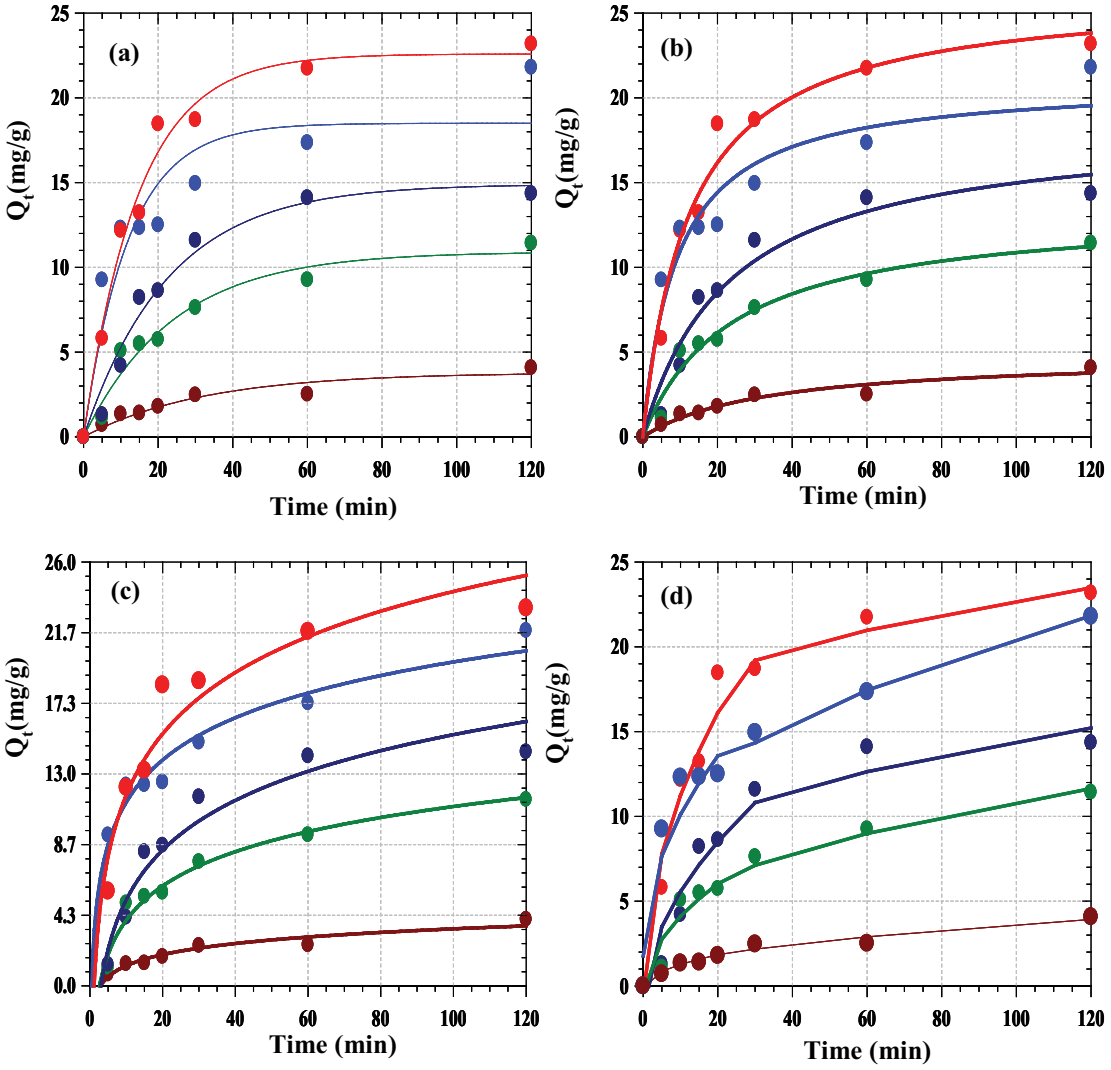

Fig. 12. Kinetic model fits for the removal of CR by Fe_3O_4-Sepiolite/C (a) pseudo-first-order, (b) pseudo-second-order, (c) Elovich, and (d) intra-particle diffusion.

of these isotherm models (Eqs. (10)–(13)) are as presented in Table 3, while the parameters from the least square fits are presented in Table 4.

Fig. 13 shows the isotherm fits for CR adsorption by Fe_3O_4-Sepiolite/C obtained through the parameters presented in Table 4. The values of R^2 obtained for isotherms parameters showed that the experimental and the theoretical data displayed a higher level of agreement. The Langmuir isotherm which proposed monolayer adsorption predicted adsorption capacities of 199.0 mg g^{-1}. The separation factor, R_L is obtained from the expression $R_L = 1/(1 + b \times C_0)$ described the adsorption process, favorable adsorption falls within the range $0 < R_L < 1$, the value obtained from the study confirmed the favourability of adsorption of CR to Fe_3O_4-Sepiolite/C. The Langmuir constant has also been related to the Gibbs free energy ($\Delta G°$) of sorption reaction as $\Delta G° = RT \ln K_L$, where K_L is $b \times Q_{max}$ [6]. The negative value of free energy indicates the feasibility of the process and the spontaneous nature of the adsorption. The Freundlich isotherm parameters confirmed the surface heterogeneity of the Fe_3O_4-Sepiolite/C, the empirical parameter, $1/n$ values is less than 1. The Temkin adsorption isotherm further confirms the earlier observation of surface heterogeneity, the value of the binding constant, a_T, suggested moderately unstable complex between the adsorbent and the dye molecule, while the b_T suggested moderately high interactions between the dye and adsorbent molecule. The value of the correlation coefficient R^2 of 0.998 is a clear indication of better fitting of Temkin isotherm. Dubinin–Radushkevich isotherm allows the estimation of the energy of adsorption on energetically heterogeneous sites. This isotherm gave the lowest R^2 of 0.993 when compared with others, still a better fitting. The value of energy obtained showed that the adsorption of CR on Fe_3O_4-Sepiolite/C. The value of mean free energy, E, given as $E = 1/\sqrt{2\beta}$ was found to be 0.239 kJ mol^{-1}, this suggests that the sorption process is physisorption and endothermic [42]. Since the value of E is less 16 kJ mol^{-1} the mechanism of the ion exchange process is film-diffusion controlled. Table 5 compares the adsorption capacity the Fe_3O_4-Sepiolite/C with

Table 2
Kinetic parameters for the adsorption CR by Fe_3O_4-Sepiolite/C

C_0 (mg L^{-1})	50.00	75.00	100.00	150.00	200.00
Pseudo-first-order kinetics model parameters					
$Q_{e,exp.}$ (mg g^{-1})	4.074	11.426	14.353	21.794	23.176
$Q_{e,cal.}$ (mg g^{-1})	3.793	10.917	14.911	18.502	22.588
k_1 (min^{-1})	0.031	0.042	0.044	0.082	0.068
R^2	0.978	0.988	0.991	0.977	0.996
%SSE	0.079	0.260	0.312	10.841	0.347
RMSE	0.099	0.180	0.197	1.164	0.208
Hybrid	1.232	0.778	0.624	2.966	0.434
Pseudo-second-order kinetics model parameter					
$Q_{e,cal.}$ (mg g^{-1})	4.806	13.459	18.484	21.022	26.304
$k_2 \times 10^3$ (g mg^{-1} min^{-1})	0.006	0.003	0.002	0.005	0.003
R^2	0.985	0.991	0.986	0.989	0.995
%SSE	0.537	4.130	17.067	0.596	9.781
RMSE	0.259	0.718	1.461	0.273	1.106
Hybrid	2.541	2.517	3.725	0.612	1.982
Elovich model's parameter					
α (mg g^{-1} min^{-1})	0.345	1.146	1.462	7.634	4.692
β (g mg^{-1})	1.017	0.330	0.227	0.268	0.184
R^2	0.985	0.994	0.985	0.996	0.991
%SSE	0.157	0.017	3.449	1.543	4.023
RMSE	0.140	0.046	0.657	0.439	0.709
Hybrid	1.798	0.188	1.910	1.007	1.328
Intra-particle diffusion model parameters					
K_{1d} (mg g^{-1} $min^{-0.5}$)	0.438	1.464	2.244	2.639	3.727
C_1 (mg g^{-1})	–0.115	–0.519	–1.531	1.768	–0.545
R^2	0.991	0.972	0.963	0.982	0.988
%SSE	0.034	0.014	0.688	1.647	1.353
RMSE	0.065	0.041	0.293	0.454	0.411
Hybrid	1.348	0.260	1.285	1.318	0.976
K_{2d} (mg g^{-1} $min^{-0.5}$)	0.320	0.825	0.804	1.370	0.782
C_2 (mg g^{-1})	0.424	2.599	6.405	6.838	14.917
R^2	0.991	0.972	0.963	0.982	0.988
%SSE	0.022	0.046	0.743	0.002	0.095
RMSE	0.053	0.076	0.305	0.016	0.109
Hybrid	0.631	0.307	0.944	0.035	0.218

others in the same category towards CR dye, it is obvious that Fe_3O_4-Sepiolite/C compares favorably with them.

3.7. Regeneration study

The selection of adsorbent required consideration of some important factors, from an economic point of view, recyclability and reusability are highly important this is because reusability lowers the cost. Reusability of Fe_3O_4-Sepiolite/C was tested after it had been removed from the medium and regenerated as earlier described [43]. From the series of recycling procedures as shown in Fig. 14, it is interesting to note that adsorbent was recovered almost completely with efficiency intact up to 8 cycles when it was reduced from 98.6% to 93.5%. This implied that the adsorbent is exceptionally recoverable with outstanding reusability, therefore, the composites are promising adsorbents and highly economical for CR removal.

3.8. Thermodynamic parameters

The temperature-dependent equilibrium adsorption was investigated and subjected to thermodynamic investigations based on the expressions below (Eqs. (14)–(16)). The adsorption equilibrium constant (K_{ad}) in terms of the adsorbate equilibrium concentration (C_e) and adsorbed

Table 3
Isotherm models applied for the adsorption of CR removal by Fe_3O_4-Sepiolite/C

Name	Model	Reference
Langmuir	$Q_{eq} = \frac{Q_{max} b C_e}{1 + b C_e}$ (10)	[38]
	Q_{eq} and Q_{max} are the amounts (mg g^{-1}) of dye adsorbed per unit mass of adsorbent and maximum adsorption capacity at equilibrium, respectively, C_e is the equilibrium concentration of adsorbate, while b (L mg^{-1}) Langmuir constant.	
Freundlich	$Q_{eq} = K_F C_e^{1/n}$ (11)	[39]
	K_F (mg g^{-1}) (L $mg^{-1})^{1/n}$ is a rough estimation of the adsorption capacity of the adsorbent, $1/n$ is the adsorption intensity.	
Temkin	$Q_e = \frac{RT}{b_T} \ln a_T C_e$ (12)	[40]
	R (J $mol K^{-1}$) is the gas constant, T (K) is absolute temperature, a_T (mg L^{-1}) is the binding constant and b_T (L g^{-1}) is related to the heat of adsorption.	
Dubinin–Radushkevich	$Q_e = Q_s e^{-\beta \varepsilon^2}$ (13)	[41,42]
	Q_s (mg g^{-1}) is the saturation capacity, β (mol J)^2 is a constant relation to adsorption energy while ε is related to the mean free energy of adsorption and given $\varepsilon = RT \ln\left(1 + \frac{1}{C_e}\right)$.	

Table 4
Isotherm parameters for the adsorption CR by Fe_3O_4-Sepiolite/C

Isotherms	Parameters	
Langmuir	Q_{max} (g mg^{-1})	199.00
	b (L mg^{-1})	0.06
	R_L	0.15
	$\Delta G°$ (kJ mol)	–6.44
	R^2	0.998
Freundlich	K_F (g mg^{-1} $L^{-1/n}$)	28.22
	$1/n$	0.45
	R^2	0.998
Temkin	b_T (J mol^{-1})	0.53
	a_T (L mg^{-1})	53.36
	R^2	0.998
Dubinin–Radushkevich	Q_s (g mg^{-1})	135.80
	β × 10^6 (mol $J^{-1})^2$	8.70
	E (kJ mol^{-1})	0.24
	R^2	0.993

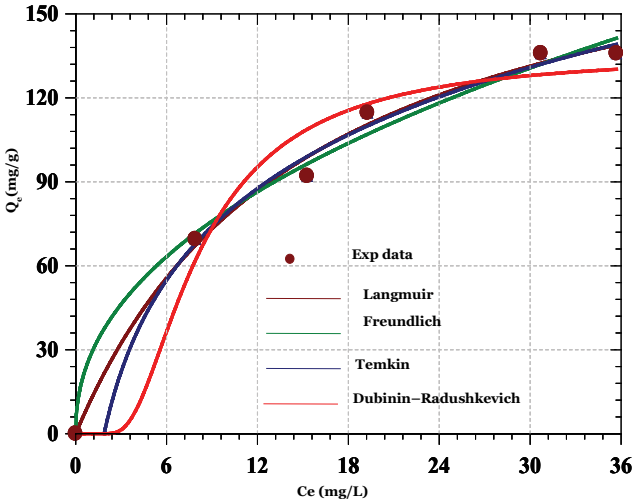

Fig. 13. Isotherm fits for the adsorption CR by Fe_3O_4-Sepiolite/C.

quantity (q_e) is expressed according to Eq. (14) at a given temperature.

$$K_{ad} = \frac{q_e}{C_e} \quad (14)$$

The Gibbs free energy change (Δ$G°$) was estimated from Eq. (15) while and the enthalpy change (Δ$H°$) and entropy change (Δ$S°$) (Table 6) were estimated from slope and intercept of the plot of lnK_{ad} vs. reciprocal of temperature (Fig. 15) [31].

$$\Delta G° = -RT \ln K_{ad} \quad (15)$$

$$\ln K_{ad} = \frac{\Delta S°}{R} - \frac{\Delta H°}{RT} \quad (16)$$

The influence of temperature on the removal of CR by Fe_3O_4-Sepiolite/C is shown in Fig. 15, as the temperature is increased from 30°C to 50°C, the removal efficiency is

Table 5
Comparison of adsorption capacity of various adsorbents for Congo red (CR) dye

Adsorbent	Adsorption capacity (mg g^{-1})	Reference
CTAB-kaolin	24.46	[43]
Natural kaolin	5.94	[43]
Natural bentonite	35.84	[44]
Kaolin	5.44	[44]
Zeolite	3.77	[44]
Organo-attapulgite	189.39	[45]
Ca-bentonite	107.41	[46]
Fe_3O_4-Sepiolite/C	199.0	This study

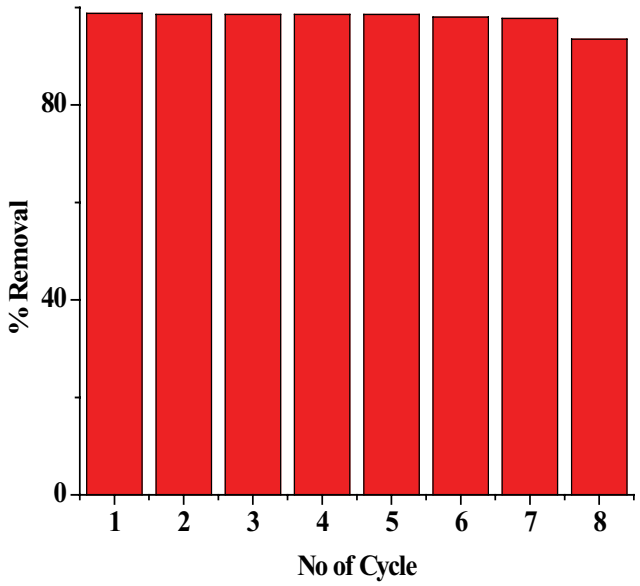

Fig. 14. Regeneration study of Fe_3O_4-Sepiolite/C.

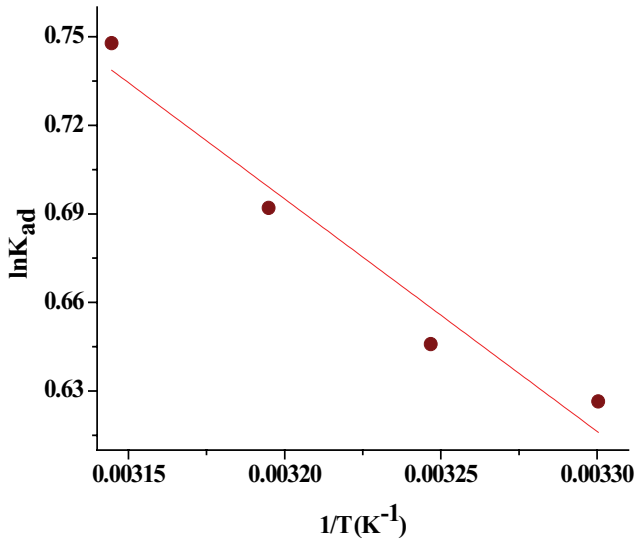

Fig. 15. $\Delta G°$ vs. temperature for the adsorption of CR by Fe_3O_4-Sepiolite/C.

Table 6
Thermodynamic parameters for the adsorption of CR by Fe_3O_4-Sepiolite/C

Temp. (K)	K_{ad}	$\ln K_{ad}$	$\Delta G°$ (J mol^{-1} K^{-1})	$\Delta H°$ (J mol^{-1} K^{-1})	$\Delta S°$ (J mol^{-1})	R^2
303	1.867	0.626	−1,578.1	6,549.35	26.74	0.932
308	1.871	0.646	−1,653.8			
313	1.908	0.692	−1,800.7			
318	1.998	0.748	−1,976.9			

increased suggesting an endothermic process as confirmed by the positive $\Delta H°$ value. The negative values of $\Delta G°$ which increase negatively with temperature shows that the process is spontaneous, while the $\Delta S°$ value suggested an increase in entropy at the solid/liquid interface during the transfer of the dye into the adsorbent [31,32].

4. Conclusion

The novel adsorbent, Fe_3O_4-Sepiolite/C was synthesized from biomass-based carbon and eco-friendly clay substance successfully. Its morphology and functional group characterization revealed a well-dispersed composite with all the component actively included. The composite was able to remove CR from aqueous solution, by adsorption process which depends on contact time, initial pollutant concentration, solution pH and adsorbent dosage. The isotherm fit well with the adsorption data with the Langmuir isotherm model having a maximum adsorption monolayer capacity of 199.0 mg g^{-1}. The kinetic data fitted well with kinetic models investigated, the results of which confirmed the isotherm suggestion that intra-particle diffusion was not the sole rate determination of the adsorption. The thermodynamic parameters for the adsorption CR by Fe_3O_4-Sepiolite/C showed that the process was endothermic and spontaneous with the negative value of Gibb's free energy. Analysis of the results of kinetics, isotherms, and recyclability confirmed Fe_3O_4-Sepiolite/C to be effective adsorbents for the removal of Congo red dye from aqueous solution.

References

[1] X. Wu, C. Liu, H. Qi, X. Zhang, J. Dai, Q. Zhang, L. Zhang, Y. Wu, X. Peng, Synthesis and adsorption properties of halloysite/carbon nanocomposites and halloysite-derived carbon nanotubes, Appl. Clay Sci., 119 (2016) 284–293.

[2] P.S. Kunwar, M. Amrita, S. Sarita, O. Priyanka, Liquid-phase adsorption of phenols using activated carbons derived from agricultural waste material, J. Hazard. Mater., 150 (2008) 626–641.

[3] K. Li, Z. Zheng, Y. Li, Characterization and lead adsorption properties of activated carbons prepared from cotton stalk by one step H_3PO_4 activation, J. Hazard. Mater., 181 (2010) 440–450.

[4] H. Demiral, E. Baykul, M. Deniz-Gezer, S. Erkoç, A. Engin, M.C. Baykul, Preparation and characterization of activated carbon from chestnut shell and its adsorption characteristics for lead, Sep. Sci. Technol., 49 (2014) 2711–2720.

[5] A. Xie, J. Dai, J. Cui, J. Lang, M. Wei, X. Dai, C. Li, Y. Yan, Novel graphene oxide–confined nanospace directed synthesis of glucose-based porous carbon nanosheets with enhanced adsorption performance, ACS Sustainable Chem. Eng., 5 (2017) 11566–11576.

[6] X. He, K.B. Male, P.N. Nesterenko, D. Brabazon, B. Paull, J.H. Luong, Adsorption and desorption of methylene blue on porous carbon monoliths and nanocrystalline cellulose, ACS Appl. Mater. Interfaces, 5 (2013) 8796–8804.

[7] M. Otero, F. Rozada, A. Morán, L. Calvo, A.I. FandGarcía, Removal of heavy metals from aqueous solution by sewage sludge based sorbents: competitive effects, Desalination, 239 (2009) 46–57.

[8] A. Salama, N. Shukry, M. El-Sakhawy, Carboxymethyl cellulose-g-poly (2-(dimethylamino) ethyl methacrylate) hydrogel as adsorbent for dye removal, Int. J. Biol. Macromol., 73 (2015) 72–75.

[9] C. Namasivayam, D. Kavitha, Removal of Congo Red from water by adsorption onto activated carbon prepared from coir pith, an agricultural solid waste, Dyes Pigm., 54 (2002) 47–58.

[10] D. Sud, G. Mahajan, M.P. Kaur, Agricultural waste material as potential adsorbent for sequestering heavy metal ions from aqueous solutions–a review, Bioresour. Technol., 99 (2008) 6017–6027.

[11] A. Demirbas, Agricultural based activated carbons for the removal of dyes from aqueous solutions: a review, J. Hazard. Mater., 167 (2009) 1–9.

[12] T.B. İyim , G. Güçlü, Removal of basic dyes from aqueous solutions using natural clay, Desalination, 249 (2009) 1377–1379.

[13] E. Errais, J. Duplay, F. Darragi, I. M'Rabet, A. Aubert, F. Huber, G. Morvan, Efficient anionic dye adsorption on natural untreated clay: kinetic study and thermodynamic parameters, Desalination, 275 (2011) 74–81.

[14] M.S.U. Rehman, M. Munir, M. Ashfaq, N. Rashid, M.F. Nazar, M. Danish, J.I. Han, Adsorption of brilliant Green dye from aqueous solution onto red clay, Chem. Eng. J., 228 (2013) 54–62.

[15] Z. Ali, M. Hussain, M. Arshad, Saccharification of corn cobs an agro-industrial waste by sulphuric acid for the production of monomeric sugars, Int. J. Biosci., 5 (2014) 204–213.

[16] UNEP, Fiduciary Responsibility: Legal and Practical Aspects of Integrating Environmental, Social and Governance Issues into Institutional Investment, UNEP FI, Geneva, 2009.

[17] Q. Wang, H. Li, L. Chen, X. Huang, Monodispersed hard carbon spherules with uniform nanopores, Carbon, 39 (2001) 2211–2214.

[18] S.H. Yu, X.J. Cui, L. Li, K. Li, B. Yu, M. Antonietti, H. Cölfen, From starch to metal/carbon hybrid nanostructures: hydrothermal metal-catalyzed carbonization, Adv. Mater., 16 (2004) 1636–1640.

[19] B. Hu, S.H. Yu, K. Wang, L. Liu, X.W. Xu, Functional carbonaceous materials from hydrothermal carbonization of biomass: an effective chemical process, Dalton Trans., 40 (2008) 5414–5423.

[20] B. Hu, K. Wang, L. Wu, S.H. Yu, M. Antonietti, M.M. Titirici, Engineering carbon materials from the hydrothermal carbonization process of biomass, Adv. Mater., 22 (2010) 813–828.

[21] M.M. Titirici, M. Antonietti, Chemistry and materials options of sustainable carbon materials made by hydrothermal carbonization, Chem. Soc. Rev., 39 (2010) 103–116.

[22] J. Gülen, Z. Altın, M. Özgür, Adsorption of amitraz on the clay, Am. J. Eng. Res., 2 (2013) 1–8.

[23] E. Sabah, M. Majdan, Removal of phosphorus from vegetable oil by acid-activated Sepiolite, J. Food Eng., 91 (2009) 423–427.

[24] E. Eren, O. Cubuk, H. Ciftci, Adsorption of basic dye from aqueous solutions by modified Sepiolite: equilibrium, kinetics and thermodynamics study, Desalination, 249 (2010) 88–96.

[25] A. Celebioglu, T. Uyar, Cyclodextrinnanofibers by electrospinning, Chem. Comun., 46 (2010) 6903–6905.

[26] M.J. Prauchner, V.M. Pasa, N.D. Molhallem, C. Otani, S. Otani, L.C. Pardini, Structural evolution of *Eucalyptus* tar pitch-based carbons during carbonization, Biomass Bioenergy, 28 (2005) 53–61.

[27] Z. Liu, F.S. Zhang, R. Sasai, Arsenate removal from water using Fe_3O_4-loaded activated carbon prepared from waste biomass, Chem. Eng. J., 160 (2010) 57–62.

[28] Q. Yu, S. Deng, G. Yu, Selective removal of perfluorooctanesulfonate from aqueous solution using chitosan-based molecularly imprinted polymer adsorbents, Water Res., 42 (2008) 3089–3097.

[29] H. Peng, H. Wang, J. Wu, G. Meng, Y. Wang, Y. Shi, Z. Liu, X. Guo, Preparation of superhydrophobic magnetic cellulose sponge for removing oil from water, Ind. Eng. Chem. Res., 55 (2016) 832–838.

[30] Y. Huang, Y. Liu, G. Zhao, J.Y. Chen, Sustainable activated carbon fiber from sawdust by reactivation for high-performance supercapacitors, J. Mater. Sci., 52 (2017) 478–488.

[31] A.I. Adeogun, E.A. Ofudje, M.A. Idowu, S.O. Kareem, S. Vahidhabanu, B.R. Babu, Biowaste-derived hydroxyapatite for effective removal of reactive yellow 4 dye: equilibrium, kinetic, and thermodynamic studies, ACS Omega, 3 (2018) 1991–2000.

[32] A.I. Adeogun, M.A. Idowu, O.K. Akiode, Biosorption and Bioremediation of Cu(II) contaminated water by *Saccharum*

officinarum: effect of oxalic acid modification on equilibrium, kinetic and thermodynamic parameters, Bioresour. Bioprocess., 3 (2016) 1–16.
[33] S. Lagergren, About the theory of so-called adsorption of soluble substances, KungligaSuenk, Vetenskapsakademiens, Handlinger Band., 24 (1889) 1–39.
[34] Y.S. Ho, W.T. Chiu, C.C. Wang, Regression analysis for the sorption isotherms of basic dyes on sugarcane dust, Bioresour. Technol., 96 (2005) 1285–1291.
[35] S.J. Elovich, in: J.H. Schulman, Ed., Proceedings of the 2nd International Congress on Surface Activity, 11, Academic Press, Inc., New York, NY, 253 (1959).
[36] W.J. Weber, J.C. Morris, Kinetics of adsorption on carbon from solution, J. Sanit. Eng. Div., 89 (1963) 31–60.
[37] I. Langmuir, The adsorption of gases on plane surfaces of glass, mica and platinum, J. Am. Chem., 40 (1918) 1361–1403.
[38] H.M. Freundlich, Uber die adsorption in lösungen, Z. Phys. Chem., 57 (1906) 385–470.
[39] M.J. Temkin, V. Pyzhev, Kinetics of ammonia synthesis on promoted iron catalysts, Acta Physiochim. URSS., 12 (1940) 217–222.
[40] M.M Dubinin, L.V. Radushkevich, Equation of the characteristic curve of the activated charcoal, Chem. Zentralbl., 1 (1947) 875–890.
[41] J.P. Hobson, Physical adsorption isotherms extending from ultrahigh vacuum to vapor pressure, J. Phys. Chem., 73 (1969) 2720–2727.
[42] Q. Wang, H. Li, L. Chen, X. Huang, Monodispersed hard carbonspherules with nanopores, Carbon, 39 (2001) 2211–2214.
[43] M. Zenasni, B. Meroufel, A. Merlin, B. George, Adsorption of Congo red from aqueous solution using CTAB-kaolin from Bechar Algeria, J. Surf. Eng. Mater. Adv. Technol., 4 (2014) 332–341.
[44] V. Vimonses, S. Lei, B. Jin, C.W.K. Chow, C. Saint, Kinetic study and equilibrium isotherm analysis of Congo Red adsorption by clay materials, Chem. Eng. J., 148 (2009) 354–364.
[45] H. Chen, J. Zhao, Adsorption study for removal of Congo red anionic dye using organo-attapulgite, Adsorption, 15 (2009) 381–389.
[46] L. Lian, L. Guo, C. Guo Adsorption of Congo red from aqueous solutions onto Ca-bentonite, J. Hazard. Mater., 161 (2009) 126–131.